MATERIALS CHEMISTRY FRONTIERS

RESEARCH ARTICLE

View Article Online
View Journal

Cite this: DOI: 10.1039/d5qm00889a

Pd@CN-COF: a pool for palladium(0)-catalyzed reactions

Marcela Horáková, [a] Milan Klikar, [a] Jakub Halamek, [b] Roman Bulánek, [b] Jhonatan Rodriguez-Pereira, [c] Veronika Čičmancová, [c] Jan Podlesný, [d] Eva Kolíbalová, [e] Jan Michalička, [e] Jan Bartáček, [a] Patrik Pařík, [a] Jan M. Macak [ce] and Filip Bureš *[a]

Received 11th December 2025,
Accepted 27th February 2026

DOI: 10.1039/d5qm00889a

rsc.li/frontiers-materials

A new cyano-substituted olefin-linked COF was synthesized and utilized as a support for palladium nanoparticles. The resulting Pd@CN-COF was demonstrated as a versatile heterogeneous catalyst in cross-coupling reactions, cyanation, and allylic substitution with the productivity exceeding the commercial homogeneous precatalyst [$Pd(PPh_3)_4$]. The catalytic activity of Pd@CN-COF was further evaluated in synthetically valuable transformations towards industrially, agrochemically, and pharmacologically relevant products.

Introduction

Ordered porous materials, especially inorganic zeolites/mesoporous silica, hybrid metal organic frameworks (MOFs), and covalent organic frameworks (COFs), play a pivotal role in modern materials science and catalysis.[1] The latter class of 2D or 3D porous organic polymers is characterized by a highly ordered and periodic structure achieved through the rational selection of building units and tailor-made synthesis.[2] Inspired by the well-established materials such as graphite and boron nitride, the first boron-based COFs were prepared by Yaghi *et al.*[3] This breakthrough achievement has initiated intense research[4] lasting two decades and resulting in the current extensive library of available COFs designed towards manifold applications.[5] Whereas the nanoscale pores in COF scaffolds provide an ideal environment for gas storage,[6] the ordered columnar arrangement enabling charge carrier transport makes COFs promising candidates for energy-storage[7] and optoelectronic[8] applications. Furthermore, the COF's high surface area is advantageous for chemical sensing[9] and catalysis.[10]

The COF-mediated heterogeneous catalysis has proven to be a versatile platform for various chemical transformations, stemming from the robust and insoluble character of COF scaffolds, ensuring stability and facile recyclability of the catalyst.[10] Moreover, the structure of organic COFs can be easily tailored to achieve the desired catalytic performance. In principle, the catalytic activity can originate from either the COF (functionalized backbone and pore walls)[11] or the COF pores may accommodate an external catalytic species such as single atoms,[12] molecules,[13] metal complexes,[14] and nanoparticles.[15] The first example of $Pd(OAc)_2$ coordinated between the COF layers reported by Wang *et al.* revealed the application potential of COFs as ligands in the Suzuki–Miyaura cross-coupling.[16] Since then, COF-supported heterogeneous catalysts have been employed in a wide range of catalytic processes, including photocatalysis[17] and electrocatalysis.[18] The current research interest focused on the COF-supported (noble) metal nanoparticles stems from their exceptional properties and catalytic performance.[19] Principally, the COFs are used to stabilize nanoparticles *via* functionalization of their surface, which inherently affects their interaction with the given substrate and thus allows modulation of the catalytic performance.[20]

Targeting robust Pd-catalysis towards valuable industrial and pharmacological products[21] and inspired by the pioneering work of Wang *et al.*[16] and the recent study by Yang *et al.*[22] (Fig. 1), we report herein the design, synthesis, and properties of a new cyano-substituted olefin-linked COF, **CN-COF**, and its application as a support for the *in situ* generated palladium nanoparticles (Pd NPs). The resulting **Pd@CN-COF** is demonstrated to act as a versatile Pd precatalyst in seven, synthetically valuable, palladium-catalyzed transformations, including various cross-coupling reactions, catalytic cyanation, and allylic substitution.

[a] *Institute of Organic Chemistry and Technology, Faculty of Chemical Technology, University of Pardubice, Studentská 573, Pardubice, 53210, Czechia. E-mail: filip.bures@upce.cz; Web: https://www.bures.upce.cz*
[b] *Department of Physical Chemistry, Faculty of Chemical Technology, University of Pardubice, Studentská 573, Pardubice, 53210, Czechia*
[c] *Center of Materials and Nanotechnologies – CEMNAT, Faculty of Chemical Technology, University of Pardubice, nám. Čs. legií 565, Pardubice, 53002, Czechia*
[d] *Institute of Technology and Business in České Budějovice, Okružní 517/10, České Budějovice, 37001, Czechia*
[e] *Central European Institute of Technology, Brno University of Technology, Purkyňova 123, Brno, 61200, Czechia*

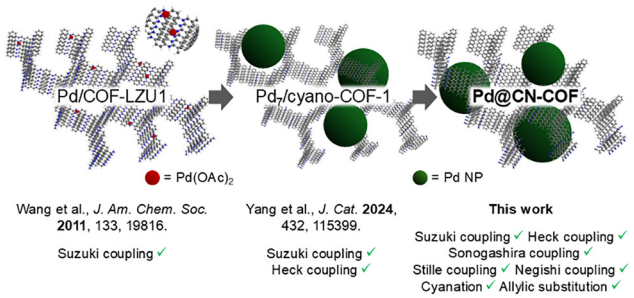

Fig. 1 Pd@COFs for Pd-catalyzed transformations.

Results and discussion

CN-COF preparation and characterization

The synthesis of **CN-COF** was performed through a Knoevenagel condensation of 1,3,5-tris(4-formylbiphenyl)-benzene (**TFBB**) and (benzene-1,3,5-triyl)triacetonitrile (**BTAN**) as outlined in Fig. 2a. Upon multiple optimization experiments using different solvents and bases (Table S1), the optimal solvothermal conditions (*ortho*-dichlorobenzene (*o*-DCB)/*n*-butanol (9 : 1) and aq. NaOH (5 M)) afforded **CN-COF** as a yellow fluffy solid with high crystallinity, bright solid-state fluorescence, and in a reproducible way (~90% yield). The model compound **MC** was obtained by reacting **TFBB** with phenylacetonitrile in the

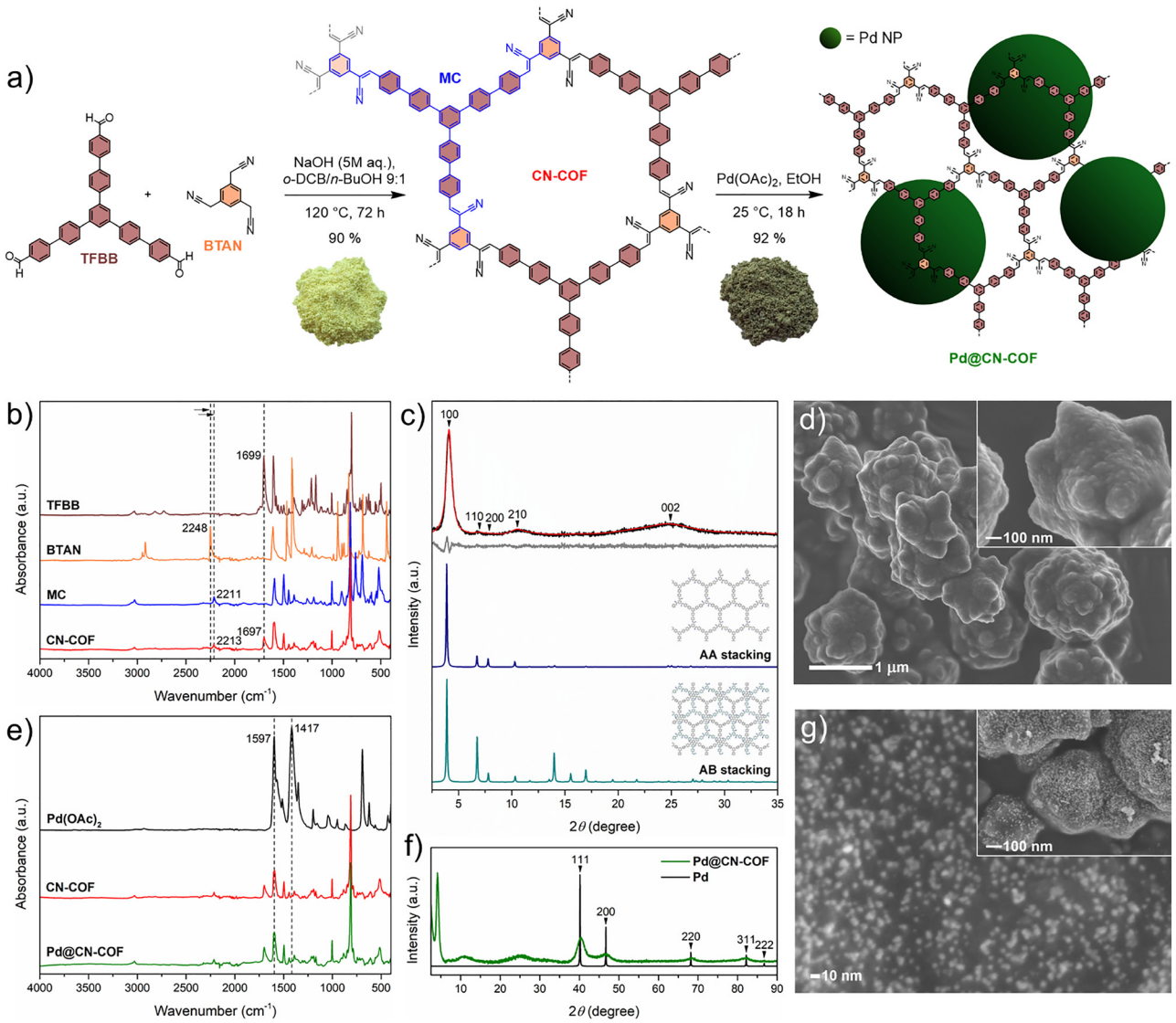

Fig. 2 (a) Synthesis of **CN-COF**, **Pd@CN-COF**, and the structure of the model compound **MC** (shown in blue), (b) a comparison of FT-IR spectra of the starting compounds (**TFBB** and **BTAN**), the model compound **MC**, and **CN-COF**, (c) experimental (black) and Le Bail refined (red) powder XRD patterns of **CN-COF**, the difference (grey), and the theoretical patterns of AA and AB stacking, (d) SEM images of **CN-COF**, (e) a comparison of FT-IR spectra of the starting Pd(OAc)$_2$ and **CN-COF** with the resulting **Pd@CN-COF**, (f) powder XRD pattern of **Pd@CN-COF** against the theoretical powder XRD pattern of Pd(0) (COD: 9008478), and (g) SEM images of **Pd@CN-COF**.

presence of KOH; see the SI for more details. The constitution and the connectivity of the novel **CN-COF** were confirmed by FT-IR, Raman, and solid-state ^{13}C CP/MAS NMR spectroscopies. As compared to **TFBB**, the FT-IR spectrum of **CN-COF** (Fig. 2b) shows a significant decrease in the intensity of the carbonyl stretching band ($\sim$1700 cm^{-1}), indicating a high degree of polymerization between the building units. This is further supported by a shift of the nitrile stretching band from 2248 (**BTAN**) to 2211/2213 cm^{-1} (**MC**/**CN-COF**), which is attributed to the conjugation of the nitrile groups with the newly formed olefinic linkages. Due to the low intensity of these FT-IR signals, we have unambiguously confirmed the presence of cyano groups also by Raman spectroscopy (Fig. S11). A very similar peak pattern was observed in the ^{13}C CP/MAS NMR spectra of **CN-COF** and **MC**, even when compared to ^{13}C NMR spectrum of **MC** in the solution (Fig. S3). The crystal structure of **CN-COF** was investigated by the powder XRD analysis (PXRD). The experimentally obtained diffractogram was optimized by the Le Bail refinement (Fig. S14 and S15) and further compared with the patterns calculated for the AA and AB stacking modes (Fig. 2c). The comparison revealed a close agreement between the observed diffraction lines at low angles ($< \sim 12^\circ$), the (100), (110), (200), and (210), of both model data sets and the experiment. At higher angles, a very broad (002) diffraction line centered at approximately 24° was experimentally observed, which corresponds to the interlayer distance of hexagonal layers. The experimentally obtained diffractogram matches well with the predicted PXRD profile of the AA stacking mode. On the contrary, the presence of no other observably large peaks at angles above $\sim 12^\circ$ (corresponding to shorter d-spacings) points to the lack of a clear presence of a well-ordered AB stacking mode, whose predicted PXRD profile contains clearly visible (101) ($\sim 14^\circ$), (201) ($\sim 15.5^\circ$), and (211) ($\sim 17^\circ$) reflections. The surface morphology of **CN-COF** studied by SEM revealed cauliflower-like aggregates (Fig. 2d), while HR-TEM analysis confirmed a layered structure (Fig. S17). A parallel STEM-EDX analysis (Fig. S18) points to a minimal amount of silicon and oxygen, indicating that contamination with silicates, eventually formed by a reaction of NaOH with the glass tube, is not significant.

Pd@CN-COF synthesis and characterization

Having verified the **CN-COF** structure and employing a suspension impregnation method carried out with Pd(OAc)$_2$/EtOH, **Pd@CN-COF** was prepared (Fig. 2a). The formed Pd NPs were trapped on the COF surface, while the process is accompanied by a visible color change from yellow to green. The stabilizing effect of the nitrile groups is presumed to prevent migration and agglomeration of the nanoparticles. This is ascribed to the out-of-plane twisting of the nitrile groups, as illustrated by computed structural models (Fig. S12), which makes them accessible for Pd coordination. In addition, the calculated electron density distribution (Fig. S13) reveals density concentrated over the nitrile groups, further supporting their role as coordination sites for Pd NPs. Provided no COF was present in the reaction mixture, only Pd black formation was observed. The Pd content in **Pd@CN-COF** was determined by ICP-MS to be around 5 wt%. When comparing the FT-IR spectra of Pd(OAc)$_2$, **CN-COF**, and **Pd@CN-COF** (Fig. 2e), the latter does not contain the characteristic bands at 1597 and 1417 cm^{-1}, confirming a successful reduction of Pd(OAc)$_2$ to Pd NPs. The incorporation of Pd NPs into the COF structure was further confirmed by the characteristic diffraction lines of Pd(0) (cubic (fcc), $Fm\bar{3}m$ (225); COD: 9008478) in the PXRD pattern of **Pd@CN-COF** (Fig. 2f) without affecting the crystallinity of the COF support. The SEM images shown in Fig. 2g confirm a spot-deposition of Pd NPs on the COF surface. The average size of Pd NPs ($\sim$3.7 nm) was estimated using the Scherrer equation based on the main (111) reflection ($\sim 40^\circ$) in the PXRD pattern of **Pd@CN-COF**. This value is consistent with the SEM observations, which reveals the presence of metal nanoparticles with an average size of 5.7 $\pm$ 1.3 nm (Fig. S16).

The surface chemical composition of **CN-COF** and **Pd@CN-COF**, analyzed by XPS, indicates the presence of C, O, N, Na, and Pd elements (Fig. S19a); see the SI for further details. The C 1s high-resolution spectra (Fig. S19b) revealed the expected signals of C=C, C–(C,H), C–N, C–O, C=O, COOH, and π–π^* shake-up satellite. The N 1s spectra (Fig. S19c) in both cases point to one chemical species (C$\equiv$N), while the signal of **Pd@CN-COF** is shifted by 0.2 eV towards lower binding energy as a result of the nitrile groups interacting with Pd atoms. The Pd 3d XPS spectrum of **Pd@CN-COF** (Fig. S19d) confirmed the presence of Pd(0) at 335.3/340.6 eV[23] along with Pd(II) at 336.8/342.1 eV[23a,24] and Pd(IV) at 338.4/343.7 eV,[25] most likely related to the corresponding surface oxides and hydroxides.

The TGA profile of **CN-COF**, supported by the DSC analysis (Fig. S20), exhibits a mass loss below 150 °C, which can be attributed to the evaporation of residual adsorbed solvents. The material then remained thermally stable up to $\sim$400 °C (T_i = 373 °C), after which gradual decomposition occurred. The thermal profile of **Pd@CN-COF** (Fig. S21) shows initial evaporation of solvents followed by a continuous weight loss. The DSC indicates an accelerated decomposition above $\sim$400 °C.

The parent **CN-COF** and the **Pd@CN-COF** catalyst exhibit porosity at the border between micro- and mesopores with the specific surface areas of 258 and 358 m^2 g^{-1} and the total pore volumes of 0.186 and 0.225 cm^3 g^{-1}. This observation contrasts with the common expectation that impregnation with metal nanoparticles leads to a decrease in the surface area. To verify the trend, repeated measurements of the pristine support and the Pd catalyst were performed, consistently confirming this anomalous behavior. Considering these findings, we suggest that the COF framework undergoes solvent-induced swelling during palladium surface-deposition, which may result in an increase in the accessible surface area. An analogous trend was reported by Platero-Prats *et al.*,[26] who observed surface areas of 550 and 664 m^2 g^{-1} for the COF and the *in situ* impregnated material, respectively. The palladium dispersion and the average size of Pd NPs in **Pd@CN-COF** were estimated using specific CO adsorption on Pd. The dispersion, according to the considered CO/Pd stoichiometry, reaches values of 18–36%, while the size of Pd NPs was 3.2–6.4 nm, in a very good

agreement with the estimations from the PXRD and SEM image analysis; see the SI for further details.

Pd@CN-COF initiated transformations

Encouraged by the recent reports on COF-based Pd catalysis[27] and considering $[Pd(PPh_3)_4]$ as a prototype Pd(0) precatalyst, we have further evaluated the catalytic performance of **Pd@CN-COF** in Pd-initiated cross-coupling reactions, cyanation, and allylic substitution (Table 1). The initial screening of solvents revealed highly polar solvents such as DMF, NMP, and ACN to be the most effective medium. Applying **Pd@CN-COF** (0.5 mol%) in a model Suzuki–Miyaura cross-coupling reaction between model bromo/iodobenzene **1**/**2** and tolylboronic acid **3** afforded 4-methylbiphenyl **4** nearly quantitatively at 25 °C and within 0.5 h. When compared with the performance of previously reported Pd(0)@COF catalysts in the Suzuki–Miyaura reaction (Table S6), **Pd@CN-COF** demonstrated an outstanding catalytic activity among them, as reflected by a rapid conversion at room temperature. A comparable performance was observed for Pd_7/cyano-COF-1 (>99% within 1 h at 25 °C),[22] suggesting that cyano-substituted COFs represent an effective support for catalytically active Pd(0), in contrast to imine-, enamine-, or hydrazone-based COFs. For the latter, elevated temperatures and longer reaction times are usually required and generally an uncomplete conversion is achieved. This can be attributed to a diffusion of reagents in/out of the COF's pores, whereas the surface-exposed catalytic sites of **Pd@CN-COF** are readily accessible for oxidative addition. Moreover, coordination of Pd NPS with the π-system and cyano groups of **CN-COF** renders the opposite face of Pd inaccessible, thereby enforcing the *cis*-orientation of the Pd(II) diaryl complex and facilitating reductive elimination. Notably, this also contrasts with $[Pd(PPh_3)_4]$ precatalyst, which required a reaction time of 3 h and failed completely in converting the iodobenzene **2**. The poor reactivity of aryl iodides in the Suzuki–Miyaura reactions employing the Pd/PPh_3 catalytic systems at lower temperatures has previously been addressed by Bissember *et al.*[28] The suggested poor turnover of the *trans*-intermediate resulting from the initial

Table 1 Pd-initiated model reactions[a]

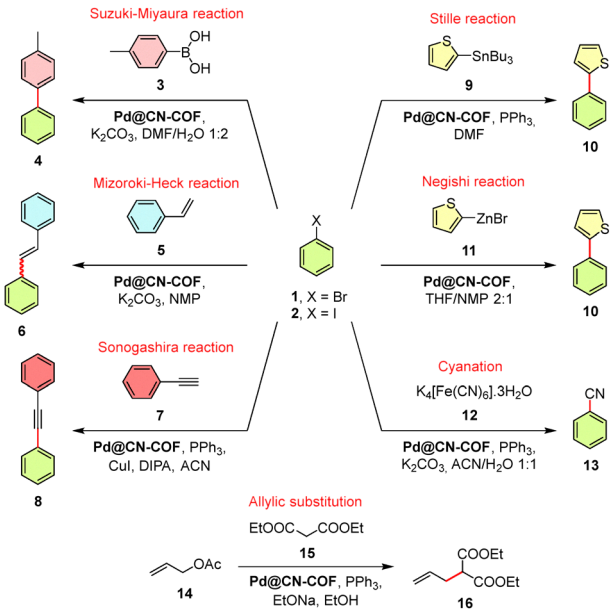

Reaction	X	Catalysis (mol%)	T (°C)	PPh_3	Pd@CN-COF		$[Pd(PPh_3)_4]$	
					t (h)	Conversion (%)	t (h)	Conversion (%)
Suzuki–Miyaura	Br	0.5	25	✗	0.5	>99	3	95
	I	0.5	25	✗	0.5	97	24	2
Mizoroki–Heck	Br	2	120	✗	24	78	3	95
	I	0.5	120	✗	4	96	3	96
Sonogashira	Br	0.5	80	✓	24	0	24	0
	I	0.5	80	✓	2.5	97	2.5	95
Stille	Br	2	80	✓	24	86	2	95
	I	0.5	80	✓	4	95	4	95
Negishi	Br	0.5	65	✗	24	60	24	61
	I	0.5	65	✗	24	87	24	90
Cyanation	Br	0.5	80	✓	24	0	24	0
	I	0.5	80	✓	10	>99	6	>99
Allylic substitution	—	0.5	50	✓	1	72	0.5	72

[a] All reactions were carried out on a 0.2 mmol scale under an argon atmosphere. The conversions were determined by GC/MS analysis.

oxidative addition of **2** was confirmed through the **Pd@CN-COF**-initiated reaction carried out in the presence of PPh_3, which resulted in a lower conversion (78%) and a significantly extended reaction time (24 h; Table S5). However, in other reactions conducted at elevated temperature, Sonogashira and cyanation in particular, a generally higher reactivity of **2** over **1** was observed. When comparing the reaction times and the achieved conversions across Table 1, both heterogeneous and homogeneous catalysis with **Pd@CN-COF** and $[Pd(PPh_3)_4]$ are comparable. The lower reactivity of **1** in the Mizoroki–Heck and Stille reactions can be enhanced by increasing the catalysis (to 2 mol%) or by raising the reaction temperature. In contrast to the Suzuki–Miyaura reaction, the further screening also indicated an enhanced catalytic performance of **Pd@CN-COF** in the presence of an additional P-ligand (PPh_3) in certain types of reactions. While the Mizoroki–Heck (Table S7) and Negishi (Table S10, X = I) reactions provided comparable results with or without PPh_3, the presence of the P-ligand proved to be crucial in the Stille reaction (Table S9, X = Br) and the cyanation (Table S11). In the Sonogashira (Table S8) and Tsuji–Trost (Table S12) reactions, the additional PPh_3 enabled full conversions within the same reaction time as those observed with $[Pd(PPh_3)_4]$. In the Negishi reaction of **1** (Table S10), a slight decrease in conversion was observed in the presence of PPh_3. Regarding byproducts, the **Pd@CN-COF**-initiated cross-coupling reactions showed minor homocoupling (<5%), none dehalogenation, prevailingly (*Z*)-**6** product in the Mizoroki–Heck reaction, and eventually two-fold allylation affording **17** (<14%, Table S12). These features are analogous to $[Pd(PPh_3)_4]$.

The reusability of **Pd@CN-COF** was examined in the Suzuki–Miyaura reaction, which revealed stable conversion over three cycles (99 to 94%) and a subsequent decrease in the catalytic activity to 61%. The **Pd@CN-COF** productivity reaches cumulative TON values up to *ca.* 890 with the cycle-TOF up to 396 h^{-1}, which can be compared with TON 190 and TOF 63.3 h^{-1} obtained for the homogeneous $[Pd(PPh_3)_4]$ (Table S15 and Fig. S43, S44). Based on the performed analysis of the used catalyst (Fig. S26–S32), this is attributed to the Pd surface site deactivation caused by adsorbed organic residues, particularly DMF, as evidenced by the infrared spectrum of the recycled **Pd@CN-COF** (Fig. S26). This is further supported by XPS analysis of the used catalyst, which revealed an increased signal of C=O and a marked reduction of Pd compared to the fresh catalyst (Fig. S30c and d). A similar ability of DMF to reduce Pd(II) towards Pd NPs has been reported by Obora *et al.*[29] Characterization of the used catalyst by adsorption of dinitrogen and CO revealed a decrease in the specific surface area (from 358 to 204 $m^2\ g^{-1}$) and the total pore volume (from 0.225 to 0.12 $cm^3\ g^{-1}$), although the pore structure remained unchanged. The CO adsorption data indicates a reduced amount of CO interacting with Pd atoms (from 1.884 to 0.234 $cm^3\ g^{-1}$), which would suggest an increase in nanoparticle size to 11–21 nm. Despite this, both PXRD and SEM analyses (Fig. S27 and S29) confirmed that the Pd NPs retained their original size, suggesting that no significant sintering has occurred. The apparent increase in nanoparticle size derived from the CO adsorption is caused by a partial blockage of the Pd surface sites by adsorbed DMF. The ICP-MS analysis reveals 4.14 wt% of Pd in the four-times recycled catalyst, indicating a minor leaching of the palladium from the initial 4.91 wt%. This finding is consistent with the Pd concentration detected in the filtrate after the first catalytic cycle, corresponding to a loss of 0.14 wt%. In the Suzuki–Miyaura reaction, repeatedly adding the reactants to the reaction mixture, while maintaining a steady amount of the catalyst (0.5 mol%), resulted in an initial quantitative conversion over 45 minutes, after which the subsequent conversion stabilized between 89–85%. This feature makes **Pd@CN-COF** a promising catalytic system for the use under continuous-flow conditions.

Practical applications of Pd@CN-COF

Having verified the catalytic behavior of our catalyst, we further address the application of **Pd@CN-COF** in the construction a key C–C bond of agrochemically, industrially, and pharmacologically relevant products **20**, **23**, **25**, **27**, and **32** (Fig. 3). Intermediate **20** is easily accessible *via* the Suzuki–Miyaura reaction of **18** and **19**, representing the first step of the industrial synthesis of boscalid,[30] a broad-spectrum carboxamide fungicide. The biphenyl **20** can be prepared nearly quantitatively and within only 2 h (Fig. 3a). Starting from iodides **21**/**24**, propargyl alcohol **22** or ethynylbenzene **7**, the catalytic performance of **Pd@CN-COF** in the Sonogashira cross-coupling reactions towards **23** and **25** is further demonstrated (Fig. 3b and c). Whereas **23** represents a synthetic precursor of justicidone, a dioxo-lignan derivative investigated for its potential biological activity,[31] the product **25** is a part of ponatinib, a tyrosine kinase inhibitor used to treat some variety of leukemia.[32]

Both products can be obtained in very good yields of 90 and 91% by using **Pd@CN-COF** catalyst. Owing to their exceptional electronic and optical properties, thiophene-based π-conjugated systems with alternating D–A–D structure (D/A ∼ electron donor/acceptor) are attractive organic semiconductors.[33] 4,7-Disubstituted benzo[*c*][1,2,5]thiadiazole (BTDA) is a prototypical example, which can be obtained from **26** *via* a two-fold Stille cross-coupling reaction. The product **27** was isolated smoothly with a 89% yield (Fig. 3d). Encouraged by these positive results, we carried out a one-pot, two-step synthesis of the heterocyclic product **32**, a core of a selective molecular sensor of Cu(II) and Hg(II) ions.[34] The Mizoroki–Heck reaction adapted to the starting 1-methylvinazene **28**, preventing hydrolysis of the cyano groups by replacing K_2CO_3 with DIPEA,[35] afforded intermediate **30**. Instead of its isolation, it was subsequently reacted with 2-iodothiophene **31** to form **32**, which was isolated with an unoptimized overall yield of 33% (Fig. 3e).

Conclusions

In summary, we have designed and prepared a new cyano-substituted olefin-linked COF and subsequently used it as a support for the *in situ* generated Pd nanoparticles. In contrast to the thermally and chemically labile $[Pd(PPh_3)_4]$, the

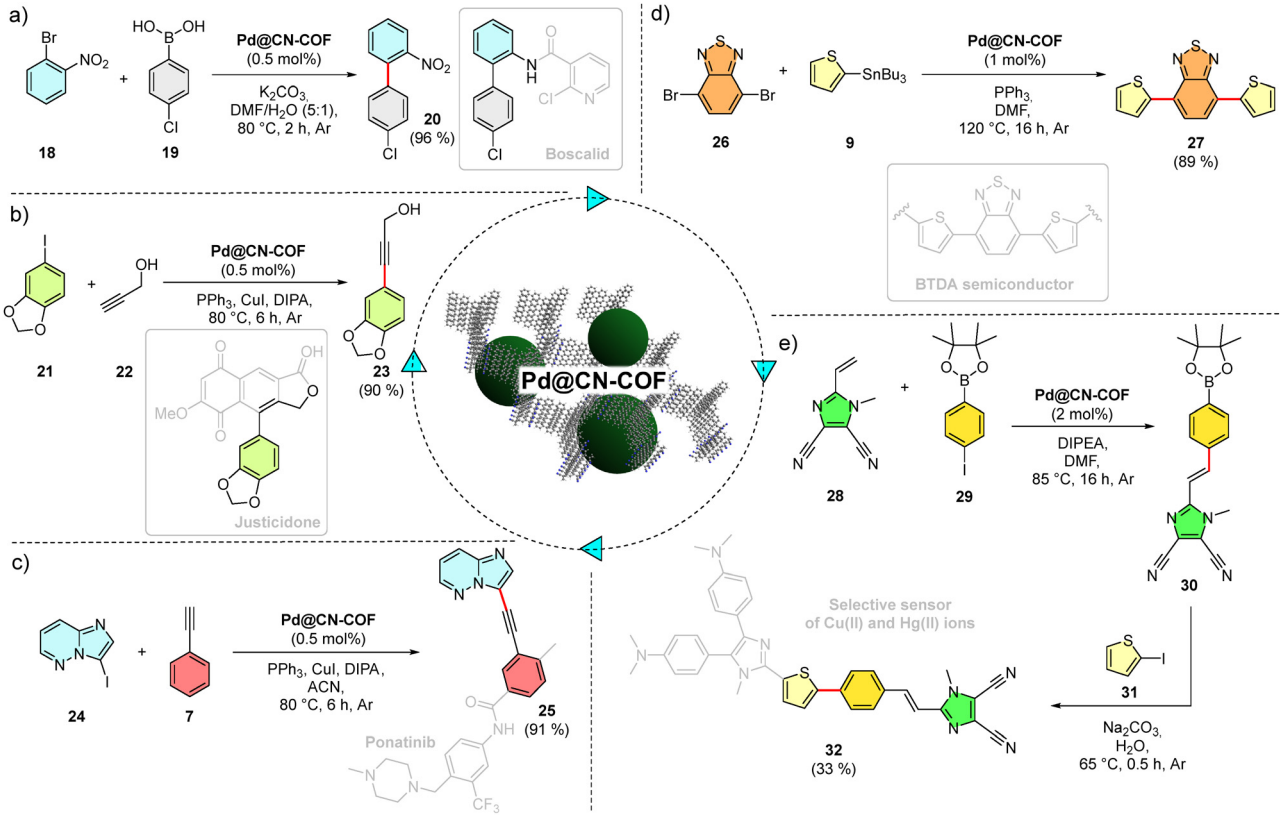

Fig. 3 Application of **Pd@CN-COF** across selected valuable transformations including Suzuki–Miyaura (a), Sonogashira (b/c), Stille (d) and Heck/Suzuki–Miyauara (e) reactions.

heterogeneous **Pd@CN-COF** is easy to prepare, proved to be bench stable, and provides comparable or better catalytic performance and thus may compete with the commercially available homogeneous Pd precatalysts.

Author contributions

Marcela Horáková: investigation, methodology, formal analysis, writing – original draft. Milan Klikar: investigation, methodology, supervision. Jakub Halamek: investigation. Roman Bulánek: investigation, writing – original draft. Jhonatan Rodriguez-Pereira: investigation. Veronika Čičmancová: investigation. Jan Podlesný: investigation. Eva Kolíbalová: investigation. Jan Michalička: investigation. Jan Bartáček: investigation. Patrik Pařík: investigation. Jan M. Macak: investigation. Filip Bureš: writing – review & editing, supervision, project administration, funding acquisition, conceptualization.

Conflicts of interest

There are no conflicts to declare.

Data availability

The data underlying this study are openly available in Figshare at **https://doi.org/10.6084/m9.figshare.30691823**.

Supplementary information (SI): syntheses and characterizations, NMR/MS/IR spectra, simulations, PXRD, microscopy images, XPS, thermal properties, volumetry, and catalysis (PDF), simulated AA stacking of CN-COF (CIF), simulated AB stacking of CN-COF (CIF). See DOI: **https://doi.org/10.1039/d5qm00889a**.

Acknowledgements

This work has been funded by a grant from the Programme Johannes Amos Comenius under the Ministry of Education, Youth and Sports of the Czech Republic [no. CZ.02.01.01/00/23_021/0008593]. The financial support from the Ministry of Education, Youth and Sports of the Czech Republic for the CEMNAT and CzechNanoLab large research infrastructures (LM2023037, LM2023051) are gratefully acknowledged for XPS, SEM and HRTEM accesses, respectively. The authors also acknowledge Dr. Matthew A. Addicoat (Nottingham Trent University) for his guidance and support in performing structural simulations.

References

1 G. S. Day, H. F. Drake, H.-C. Zhou and M. R. Ryder, Evolution of porous materials from ancient remedies to modern frameworks, *Commun. Chem.*, 2021, **4**, 114; A. Thomas,

Much ado about nothing – a decade of porous materials research, *Nat. Commun.*, 2020, **11**, 4985.

2 P. J. Waller, F. Gándara and O. M. Yaghi, Chemistry of Covalent Organic Frameworks, *Acc. Chem. Res.*, 2015, **48**, 3053–3063.

3 A. P. Côté, A. I. Benin, N. W. Ockwig, M. O'Keeffe, A. J. Matzger and O. M. Yaghi, Porous, Crystalline, Covalent Organic Frameworks, *Science*, 2005, **310**, 1166–1170.

4 K. Geng, T. He, R. Liu, S. Dalapati, K. T. Tan, Z. Li, S. Tao, Y. Gong, Q. Jiang and D. Jiang, Covalent Organic Frameworks: Design, Synthesis, and Functions, *Chem. Rev.*, 2020, **120**, 8814–8933; M. S. Lohse and T. Bein, Covalent Organic Frameworks: Structures, Synthesis, and Applications, *Adv. Funct. Mater.*, 2018, **28**, 1705553.

5 R. Liu, K. T. Tan, Y. Gong, Y. Chen, Z. Li, S. Xie, T. He, Z. Lu, H. Yang and D. Jiang, Covalent organic frameworks: an ideal platform for designing ordered materials and advanced applications, *Chem. Soc. Rev.*, 2021, **50**, 120–242.

6 Y. Yin, Y. Zhang, X. Zhou, B. Gui, W. Wang, W. Jiang, Y.-B. Zhang, J. Sun and C. Wang, Ultrahigh–surface area covalent organic frameworks for methane adsorption, *Science*, 2024, **386**, 693–696; H. Furukawa and O. M. Yaghi, Storage of Hydrogen, Methane, and Carbon Dioxide in Highly Porous Covalent Organic Frameworks for Clean Energy Applications, *J. Am. Chem. Soc.*, 2009, **131**, 8875–8883.

7 S. Kandambeth, V. S. Kale, O. Shekhah, H. N. Alshareef and M. Eddaoudi, 2D Covalent-Organic Framework Electrodes for Supercapacitors and Rechargeable Metal-Ion Batteries, *Adv. Energy Mater.*, 2021, **12**, 2100177.

8 N. Keller and T. Bein, Optoelectronic processes in covalent organic frameworks, *Chem. Soc. Rev.*, 2021, **50**, 1813–1845.

9 Z. Meng and K. A. Mirica, Covalent organic frameworks as multifunctional materials for chemical detection, *Chem. Soc. Rev.*, 2021, **50**, 13498–13558.

10 Z. Alsudairy, N. Brown, A. Campbell, A. Ambus, B. Brown, K. Smith-Petty and X. Li, Covalent organic frameworks in heterogeneous catalysis: recent advances and future perspective, *Mater. Chem. Front.*, 2023, **7**, 3298–3331.

11 A. Basak, S. Karak and R. Banerjee, Covalent Organic Frameworks as Porous Pigments for Photocatalytic Metal-Free C–H Borylation, *J. Am. Chem. Soc.*, 2023, **145**, 7592–7599; F. Meng, S. Bi, Z. Sun, D. Wu and F. Zhang, 2,4,6-Trimethylpyridine-Derived Vinylene-Linked Covalent Organic Frameworks for Confined Catalytic Esterification, *Angew. Chem., Int. Ed.*, 2022, **61**, e202210447; B. Hou, S. Yang, K. Yang, X. Han, X. Tang, Y. Liu, J. Jiang and Y. Cui, Confinement-Driven Enantioselectivity in 3D Porous Chiral Covalent Organic Frameworks, *Angew. Chem., Int. Ed.*, 2021, **60**, 6086–6093.

12 J.-M. Seo, H.-J. Noh, J.-P. Jeon, H. Kim, G.-F. Han, S. K. Kwak, H. Y. Jeong, L. Wang, F. Li and J.-B. Baek, Conductive and Ultrastable Covalent Organic Framework/Carbon Hybrid as an Ideal Electrocatalytic Platform, *J. Am. Chem. Soc.*, 2022, **144**, 19973–19980.

13 Y. Zheng, S. Zhang, J. Guo, R. Shi, J. Yu, K. Li, N. Li, Z. Zhang and Y. Chen, Green and Scalable Fabrication of High-Performance Biocatalysts Using Covalent Organic Frameworks as Enzyme Carriers, *Angew. Chem., Int. Ed.*, 2022, **61**, e202208744; H. Lyu, C. S. Diercks, C. Zhu and O. M. Yaghi, Porous Crystalline Olefin-Linked Covalent Organic Frameworks, *J. Am. Chem. Soc.*, 2019, **141**, 6848–6852.

14 Z. Fu, X. Wang, A. M. Gardner, X. Wang, S. Y. Chong, G. Neri, A. J. Cowan, L. Liu, X. Li, A. Vogel, R. Clowes, M. Bilton, L. Chen, R. S. Sprick and A. I. Cooper, A stable covalent organic framework for photocatalytic carbon dioxide reduction, *Chem. Sci.*, 2020, **11**, 543–550.

15 C. Chandran, H. D. Singh, L. S. Leo, P. Shekhar, D. Rase, D. Chakraborty, C. P. Vinod and R. Vaidhyanathan, A covalent organic framework with electrodeposited copper nanoparticles – a desirable catalyst for the Ullmann coupling reaction, *J. Mater. Chem. A*, 2022, **10**, 15647–15656; P. Pachfule, S. Kandambeth, D. D. Díaz and R. Banerjee, Highly stable covalent organic framework–Au nanoparticles hybrids for enhanced activity for nitrophenol reduction, *Chem. Commun.*, 2014, **50**, 3169–3172; P. Pachfule, M. K. Panda, S. Kandambeth, S. M. Shivaprasad, D. D. Díaz and R. Banerjee, Multifunctional and robust covalent organic framework-nanoparticle hybrids, *J. Mater. Chem. A*, 2014, **2**, 7944–7952.

16 S.-Y. Ding, J. Gao, Q. Wang, Y. Zhang, W.-G. Song, C.-Y. Su and W. Wang, Construction of Covalent Organic Framework for Catalysis: Pd/COF-LZU1 in Suzuki–Miyaura Coupling Reaction, *J. Am. Chem. Soc.*, 2011, **133**, 19816–19822.

17 B. Mishra, A. Alam, A. Chakraborty, B. Kumbhakar, S. Ghosh, P. Pachfule and A. Thomas, Covalent Organic Frameworks for Photocatalysis, *Adv. Mater.*, 2024, 2413118.

18 J.-D. Feng, W.-D. Zhang and Z.-G. Gu, Covalent Organic Frameworks for Electrocatalysis: Design, Applications, and Perspectives, *ChemPlusChem*, 2024, **89**, e202400069.

19 T. S. Rodrigues, A. G. M. da Silva and P. H. C. Camargo, Nanocatalysis by noble metal nanoparticles: controlled synthesis for the optimization and understanding of activities, *J. Mater. Chem. A*, 2019, **7**, 5857–5874.

20 L. Liu and A. Corma, Metal Catalysts for Heterogeneous Catalysis: From Single Atoms to Nanoclusters and Nanoparticles, *Chem. Rev.*, 2018, **118**, 4981–5079.

21 J. Rayadurgam, S. Sana, M. Sasikumar and Q. Gu, Palladium catalyzed C–C and C–N bond forming reactions: an update on the synthesis of pharmaceuticals from 2015–2020, *Org. Chem. Front.*, 2021, **8**, 384–414; P. Devendar, R.-Y. Qu, W.-M. Kang, B. He and G.-F. Yang, Palladium-Catalyzed Cross-Coupling Reactions: A Powerful Tool for the Synthesis of Agrochemicals, *J. Agric. Food Chem.*, 2018, **66**, 8914–8934.

22 R. Tao, B. Feng, C. Wang, H. Zhang, R. Chen, K. Liu, J. Li, X. Deng, J. Li and Y. Yang, Feasible preparation of preferentially oriented (111) Pd nanocrystals supported on cyano-COFs for ultrahigh activity in C–C cross-couplings, *J. Catal.*, 2024, **432**, 115399.

23 (*a*) B. Bawab, S. M. Thalluri, J. Rodriguez-Pereira, H. Sopha, R. Zazpe and J. M. Macak, Anodic TiO_2 nanotube layers decorated by Pd nanoparticles using ALD: an efficient electrocatalyst for methanol oxidation, *Electrochim. Acta*,

2022, **429**, 141044; (*b*) C. M. Schott, J. Holl, R. Zazpe, M. Kopp, O. Man, S. M. Thalluri, J. Rodriguez-Pereira, P. M. Schneider, K.-T. Song, E. Keles, P. Peljo, J. J. Jasielec, E. L. Gubanova, J. M. Macak and A. S. Bandarenka, Revealing Catalytic Properties of Palladium/Gold Systems toward Hydrogen Evolution, Oxidation, and Absorption with Scanning Electrochemical Microscopy, *ACS Catal.*, 2025, **15**, 9035–9046.

24 T. L. Barr, Recent advances in X-ray photoelectron spectroscopy studies of oxides, *J. Vac. Sci. Technol., A*, 1991, **9**, 1793–1805.

25 B. Bawab, S. M. Thalluri, E. Kolíbalová, R. Zazpe, L. Jelínek, J. Rodriguez-Pereira and J. M. Macak, Synergistic effect of Pd single atoms and nanoparticles deposited on carbon supports by ALD boosts alkaline hydrogen evolution reaction, *Chem. Eng. J.*, 2024, **482**, 148959.

26 I. Romero-Muñiz, A. Mavrandonakis, P. Albacete, A. Vega, V. Briois, F. Zamora and A. E. Platero-Prats, Unveiling the Local Structure of Palladium Loaded into Imine-Linked Layered Covalent Organic Frameworks for Cross-Coupling Catalysis, *Angew. Chem., Int. Ed.*, 2020, **59**, 13013–13020.

27 H. Salemi, M. Debruyne, V. Van Speybroeck, P. Van Der Voort, M. D'hooghe and C. V. Stevens, Covalent organic framework supported palladium catalysts, *J. Mater. Chem. A*, 2022, **10**, 20707–20729.

28 C. C. Ho, A. Olding, J. A. Smith and A. C. Bissember, Nuances in Fundamental Suzuki–Miyaura Cross-Couplings Employing $[Pd(PPh_3)_4]$: Poor Reactivity of Aryl Iodides at Lower Temperatures, *Organometallics*, 2018, **37**, 1745–1750.

29 J. Ishida, M. Nakatsuji, T. Nagata, H. Kawasaki, T. Suzuki and Y. Obora, Synthesis and Characterization of *N*,*N*-Dimethylformamide-Protected Palladium Nanoparticles and Their Use in the Suzuki–Miyaura Cross-Coupling Reaction, *ACS Omega*, 2020, **5**, 9598–9604.

30 I. Volovych, M. Neumann, M. Schmidt, G. Buchner, J.-Y. Yang, J. Wölk, T. Sottmann, R. Strey, R. Schomäcker and M. Schwarze, A novel process concept for the three step Boscalid® synthesis, *RSC Adv.*, 2016, **6**, 58279–58287.

31 C. J. Boluda, H. López, J. A. Pérez and J. M. Trujillo, First Total Synthesis of Justicidone, a *p*-Quinone-Lignan Derivative from *Justicia hyssopifolia*, *Chem. Pharm. Bull.*, 2005, **53**, 930–933.

32 L. Han, Y. Yu, P. Deng, S. Wang, J. Hu, S. Wang, J. Zheng, J. Jiang, Y. Dang, R. Long and Z. Gan, Design, synthesis, and biological evaluation of Ponatinib-based *N*-Phenylpyrimidine-2-amine derivatives as novel fibroblast growth factor receptor 4 (FGFR4) selective inhibitors, *Eur. J. Med. Chem.*, 2025, **284**, 117206.

33 F. Zhang, D. Wu, Y. Xu and X. Feng, Thiophene-based conjugated oligomers for organic solar cells, *J. Mater. Chem.*, 2011, **21**, 17590–17600.

34 N. Dey, J. Kulhánek, F. Bureš and S. Bhattacharya, Simultaneous Detection of Cu^{2+} and Hg^{2+} via Two Mutually Independent Sensing Pathways of Biimidazole Push–Pull Dye, *J. Org. Chem.*, 2019, **84**, 1787–1796.

35 J. Kulhánek, F. Bureš, O. Pytela, T. Mikysek and J. Ludvík, Imidazole as a Donor/Acceptor Unit in Charge-Transfer Chromophores with Extended π-Linkers, *Chem. – Asian J.*, 2011, **6**, 1604–1612.

